# NUMERICAL METHODS FOR THE SIMULATION OF CONTINUOUS SEDIMENTATION IN IDEAL CLARIFIER-THICKENER UNITS

R. BÜRGER[A], K.H. KARLSEN[B], N.H. RISEBRO[C], AND J.D. TOWERS[D]

Abstract. We consider a model of continuous sedimentation. Under idealizing assumptions, the settling of the solid particles under the influence of gravity can be described by the initial value problem for a nonlinear hyperbolic partial differential equation with a flux function that depends discontinuously on height. The purpose of this contribution is to present and demonstrate two numerical methods for simulating continuous sedimentation: a front tracking method and a finite finite difference method. The basic building blocks in the front tracking method are the solutions of a finite number of certain Riemann problems and a procedure for tracking local collisions of shocks. The solutions of the Riemann problems are recalled herein and the front tracking algorithm is described. As an alternative to the front tracking method, a simple scalar finite difference algorithm is proposed. This method is based on discretizing the spatially varying flux parameters on a mesh that is staggered with respect to that of the conserved variable, resulting in a straightforward generalization of the well-known Engquist-Osher upwind finite difference method. The result is an easily implemented upwind shock capturing method. Numerical examples demonstrate that the front tracking and finite difference methods can be used as efficient and accurate simulation tools for continuous sedimentation. The numerical results for the finite difference method indicate that discontinuities in the local solids concentration are resolved sharply and agree with those produced by the front tracking method. The latter is free of numerical dissipation, which leads to sharply resolved concentration discontinuities, but is more complicated to implement than the former. Available mathematical results for the proposed numerical methods are also briefly reviewed.

## 1. Introduction

We consider a model of continuous sedimentation of ideal suspensions of small solid particles dispersed in a viscous fluid. It is well known that under idealizing assumptions, the settling of the solid particles under the influence of gravity can be described by the one-dimensional kinematic sedimentation theory formulated by Kynch (1952). This theory models the suspension as a mixture of two superimposed continuous media, the solid and the fluid. Its essential assumption states that if $v_{\mathrm{s}}$ and $v_{\mathrm{f}}$ denote the solid and fluid phase velocity, then the relative velocity of the solids with respect to the fluid, $v_{\mathrm{r}} = v_{\mathrm{s}} - v_{\mathrm{f}}$, is a function of the local solids concentration $u$ only, $v_{\mathrm{r}} = v_{\mathrm{r}}(u)$. This assumption is well justified for suspensions of small rigid spheres showing no floc structure or compressibility effects. Recent extensive discussions of Kynch's and related sedimentation models are provided by Bustos *et al.* (1999) and Bürger and Wendland (2001).

The basic balance equations are the continuity equations of the solid and of the fluid,

$$u_t + (uv_{\mathrm{s}})_x = 0, \tag{1.1}$$

$$u_t - \big((1-u)v_{\mathrm{f}}\big)_x = 0, \tag{1.2}$$

*Date*: October 8, 2001.

*Key words and phrases.* continuous sedimentation, conservation law, discontinuous flux, weak solution, front tracking, finite difference method, convergence, numerical example.

[A]Institute of Mathematics A, University of Stuttgart, Pfaffenwaldring 57, D-70569 Stuttgart, Germany. E-Mail: buerger@mathematik.uni-stuttgart.de.

[B]Department of Mathematics, University of Bergen, Johs. Brunsgt. 12, N–5008 Bergen, Norway. E-Mail: kennethk@mi.uib.no.

[C]Department of Mathematics, University of Oslo, P.O. Box 1053, Blindern, N–0316 Oslo, Norway. E-Mail: nilshr@math.uio.no.

[D]MiraCosta College, 3333 Manchester Avenue, Cardiff-by-the-Sea, CA 92007-1516, USA. E-Mail: jtowers@cts.com.

where $t$ is time, the vertical coordinate $x$ is assumed to increase in the direction downwards, and the subscripts $t$ and $x$ denote partial derivatives. In terms of the volume-average velocity of the mixture

$$q = uv_{\mathrm{s}} + (1-u)v_{\mathrm{f}},$$

the continuity equation of the mixture, obtained as the difference of (1.1) and (1.2), can be written as $q_x = 0$, i.e., $q(\cdot,t)$ is a constant function for each $t$ and is determined by boundary and feed conditions. In particular, $q \equiv 0$ in a closed settling column without in- or outlets.

In terms of the velocities $v_{\mathrm{r}}(u)$ and $q = q(x,t)$, Eq. (1.1) can be rewritten as

$$u_t + \big(q(x,t)u + u(1-u)v_{\mathrm{r}}(u)\big)_x = 0.$$

Defining the Kynch batch flux density function $h(u) = u(1-u)v_{\mathrm{r}}(u)$, we can rewrite the governing equation in the form

$$u_t + \big(q(x,t)u + h(u)\big)_x = 0. \tag{1.3}$$

The function $h$ reflects the material properties of the suspension, and is related to the function $f_{\mathrm{bk}}$ used elsewhere by $h(u) = -f_{\mathrm{bk}}(u)$. Experiments aiming at determining the function $h$ have been conducted repeatedly (Tory 1961, Shannon *et al.* 1963, Davis *et al.* 1991, Chang *et al.* 1997). The basic assumptions on $h$ can be stated as $h(u) = 0$ for $u \le 0$ and $u \ge 1$, $h(u) > 0$ for $0 < u < 1$, $h'(0) > 0$ and $h'(1) \le 0$. We have chosen the value "1" as the maximum solids concentration and simply assume $h$ to be sufficiently smooth. The vast majority of Kynch batch flux density functions $h$ determined from settling experiments in the literature have at least one inflection point (Bustos *et al.* 1999, Bürger and Tory 2000).

A very simple model for continuous sedimentation was studied by Bustos *et al.* (1990) (see also Concha and Bustos, 1992), in which Eq. (1.3) is restricted to a space interval, say $x \in [0,1]$, corresponding to a cylindrical vessel, and where the upper end $x = 0$ is identified with a feed inlet and the lower $x = 1$ with a discharge outlet. The vessel is assumed to be fed continuously with feed suspension at the inlet (surface source) and to be discharged continuously through the outlet (surface sink). The overflow of clear liquid is not explicitly modeled. The volume average velocity is a function of time only, $q(t) = q_r(t)$, where $q_r$ is a prescribed control function determined by the discharge opening. In the model by Bustos *et al.* (1990), Eq. (1.3) is provided with Dirichlet boundary conditions at $x = 0$ and $x = 1$, i.e., one intends to prescribe boundary concentrations $u(1,t) = \phi_1(t)$ and $u(0,t) = \phi_0(t)$ at the feed and discharge levels, respectively. However, these boundary conditions are overly restrictive in that they ignore that the solution values propagate along characteristic curves (straight lines in the case of cylindrical vessels) and might intersect the boundaries of the computational domain from the interior. This occurs when the vessel, frequently referred to as *Ideal Continuous Thickener* (Shannon *et al.* 1966) empties or overflows. A mathematically appropriate reformulation of the boundary conditions, which correctly takes into account these situations, is provided by the concept of entropy boundary conditions (Bustos *et al.* 1996).

This model, which was proposed first by Petty (1975), has some severe shortcomings despite its amenability to mathematical analysis. Among them is the lack of a global conservation principle due to the use of Dirichlet boundary conditions. It is preferable to replace the boundary conditions at the ends of the vessel by transitions between the transport flux $q(x,t)u$ and the composite flux $q(x,t)u + h(u)$, such that the problem is reduced to a pure initial value problem. Moreover, in a realistic model the feed suspension should enter at a feed level located between the overflow outlet at the top and the discharge outlet at the bottom. This gives rise to an upwards-directed volume average velocity $q_l \le 0$ above and a downwards-directed velocity $q_r \ge 0$ below the feed level. The feed source itself is modeled by a singular source term. Such configurations were proposed by several authors (Lev *et al.* 1986, Severin 1991, Barton *et al.* 1992, Chancelier *et al.* 1994, Concha *et al.* 1995) under different names such as clarifier-thickener units or high-capacity thickeners. Particularly thorough analyses of clarifier-thickener models were presented by Diehl in a series of papers (Diehl 1995, 1996, 1997, 2000, 2001).

It is such an improved "clarifier-thickener" model which is considered in this paper. Its main purpose is to provide numerical methods that can be employed to simulate continuous sedimentation by computing approximate solutions of an initial value problem for a hyperbolic conservation law of the form

$$u_t + g(x,u)_x = 0, \qquad -\infty < x < \infty,\ t > 0. \tag{1.4}$$

Here we make the non-standard assumption that the flux function $g$ depends discontinuously on the spatial variable $x$ (details are given in the next section). To put the present work in the proper perspective, we remark that Bürger *et al.* (2001) demonstrated that there exists a solution to the clarifier-thickener model (i.e., the initial value problem for (1.4)). In this contribution, we describe and demonstrate numerical algorithms by which approximate solutions to such models can actually be computed. The choice of the numerical algorithms is guided by the theoretical analysis (given elsewhere), which shows that they converge to the solution of the underlying model as the repsective discretization parameters tend to zero (which, of course, is a highly desirable feature). Included in our discussion here are a front tracking method and a simple finite difference method. Both these methods have a solid theoretical foundation. The front tracking method is very accurate since it does not contain any numerical dissipation due to the use of an exact solver for Riemann problems of two scalar equations in two unknown variables ("$2 \times 2$ Riemann problems"). In particular, shock waves (i.e., admissible discontinuities in the local solids concentration) are accurately resolved. Moreover, the front tracking method is unconditionally stable in the sense that the time step is not restricted by the spatial discretization. The finite difference method, on the other hand, contains numerical dissipation. Consequently, discontinuous waves may be (slightly) smeared out. Also there is a time step restriction (the so-called CFL condition) since the method considered here is explicit. However, compared with the front tracking method, the finite difference method is very easy to implement.

The remaining part of this contribution is organized as follows. In Section 2 we provide non-technical discussions of the front tracking and finite difference methods. In Section 3 the mathematical clarifier-thickener model is described. The front tracking and finite difference methods are described in detail in Sections 4 and 5, respectively. The performance of the numerical methods are demonstrated in Section 6. Conclusions are summarized in Section 7.

## 2. The front tracking and finite difference methods

The objective of this paper is to demonstrate that numerical methods which have arisen from very recent research in the analysis and numerics of conservation laws with discontinuous fluxes provide a tool for the efficient simulation of clarifier-thickener units. In this setion we recall the general mathematical background and some recent advances for both the front tracking and finite difference methodologies. Their specific applications to the clarifier-thickener model, together with the necessary technical details, are considered in Sections 4 and 5, respectively.

### 2.1. The front tracking method.

The main idea behind by the front tracking method was introduced by Dafermos (1972). To illustrate it, consider the hyperbolic conservation law

$$\begin{aligned} u_t + \phi(u)_x = 0, &\quad -\infty < x < \infty,\ t > 0, \\ u(x,0) = u_0(x), &\quad -\infty < x < \infty, \end{aligned} \tag{2.1}$$

where the initial function $u_0$ is assumed to be piecewise constant and $\phi$ is a given flux function. Then the entropy solution can be constructed by a superposition of solutions of Riemann problems, i.e., solutions of the conservation law with initial data consisting of two constant states separated by a simple discontinuity. If the flux function $\phi$ is piecewise linear, each Riemann solution consists exclusively of constant states separated by shocks. When waves from neighboring Riemann problems interact, the interaction will only involve constant states and therefore leads to new Riemann problems and the construction can be continued forward in time. Thus, the construction consists of *solving Riemann problems* and *tracking straight-line discontinuities*. In the general case, the initial function $u_0$ is approximated by a step function and the flux $\phi$ by a piecewise linear function. In this way rarefaction waves are approximated by a sequence of small shocks. Variants of the method have been used by many authors, see Holden and Risebro (2001) for the

history and many references. In particular, Holden *et al.* (1988) proved that the construction is well-defined and terminates in a finite number of steps, even for non-convex flux functions, given a finite number of constant states in $u_0(x)$. Front tracking was later formulated for hyperbolic systems by DiPerna (1976), Bressan (1992) and Risebro (1993). Variants of the front tracking technique based on Dafermos paper (1972) have also been used earlier to compute approximate solutions to batch sedimentation problems, see Kunik (1992, 1993), Kunik *et al.* (1993) and Bustos and Concha (1999). However, to apply front tracking to the advanced clarifier-thickener model with continuous flow, one must be able to solve Riemann problems that are nonstandard in that changes between flux functions, depending on the space coordinate $x$, are involved. Such solutions were constructed by Gimse and Risebro (1990, 1992). Gimse and Risebro (1990) showed that under some mild conditions, Riemann problems with a discontinuous flux functions always have weak solutions. Furthermore, one can always single out a unique weak solution a being the limit of a viscous approximation.

A convergence proof for the front tracking method for the clarifier-thickener model is given in Bürger *et al.* (2001).

2.2. **The finite difference method.** The suggested finite difference algorithm is derived by slightly modifying the standard Engquist and Osher upwind scheme (Engquist and Osher, 1980) in order to handle the spatial variation of the flux appearing in the initial value problem for (1.4). The essential idea is to regard the spatially varying flux $g(x,u)$ as a function of $u$ and a pair of spatially varying parameters, i.e., $g(x,u) = G(\gamma^1(x), \gamma^2(x), u)$. Then the flux parameter vector $(\gamma^1(x), \gamma^2(x))$ is discretized on a spatial mesh that is staggered with respect to that of the solids concentration $u$. Since the discretization of $\gamma$ is staggered against that of the conserved quantity $u$, we can avoid solving the full $2 \times 2$ Riemann problem that would arise at each cell boundary if the two discretizations were aligned (non-staggered). The result is a scalar finite difference scheme in conservation form that incorporates a straightforward generalization of the Engquist-Osher numerical flux first proposed by Engquist and Osher (1980). With the Engquist-Osher flux, the resulting algorithm is a so-called upwind scheme, meaning that the flux differencing is biased in the direction of incoming waves, making it possible to resolve shocks without excessive smearing. The choice of the Engquist-Osher flux is also motivated by its close functional relationship to the so-called Kružkov entropy flux $F(\gamma,u) = \operatorname{sign}(u-c)\,(G(\gamma,u) - G(\gamma,c))$ (Kružkov, 1970) and the nonlinear singular function $\Psi_{\mathrm{fd}}(\gamma,u)$ to be introduced in Section 5. The relationships can be used to prove convergence for the sequence of numerical approximations. For standard (constant parameter) conservation laws, the Engquist-Osher algorithm is well known to converge to the correct entropy solution. That setting is covered by the now classical theory of monotone schemes as developed by Crandall and Majda (1980) or Harten *et al.* (1976). In particular, the numerical approximations converge to the unique entropy solution as the discretization parameters $\Delta x$ and $\Delta t$ approach zero, as long as a suitable CFL condition is enforced. For the case of a single discontinuous parameter the modified Engquist-Osher scheme was proven to converge for the case of a concave flux in Towers (2000) and for a flux with any finite number of critical points in Towers (2001). Karlsen *et al.* (2001) extended the scheme so that it would apply to degenerate parabolic equations with discontinuities in the convective flux, and established convergence to a weak solution.

A future paper is devoted to the convergence proof for the finite difference method for the clarifier-thickener model, i.e., the case of two discontinuous parameters.

## 3. The clarifier-thickener model

Consider the configuration of Figure 1, where $x = -1$, 0 and 1 are assumed to be the levels at which in normal operation, the clarified liquid leaves the equipment (overflow level), the feed suspension in pumped into the unit (feed level), and through which the concentrated sediment leaves the thickener (discharge level), respectively. At $x = 0$, the vessel is fed with fresh suspension at a volume flow rate $Q_{\mathrm{F}}(t) \geq 0$. The volume flow rate of the discharge, $Q_r(t) \geq 0$ or equivalently $q_r(t) = Q_r(t)/S$, where $S$ denotes the constant cross-sectional area of the vessel, is also prescribed.

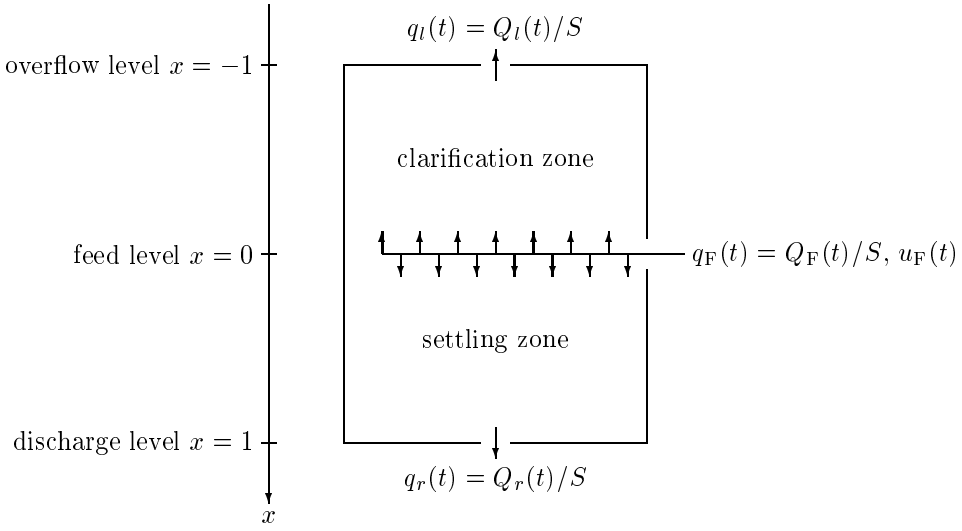


FIGURE 1. The one-dimensional clarifier-thickener model.

The volumetric balance of the mixture requires that at any time

$$Q_r(t) = Q_l(t) + Q_F(t). \tag{3.1}$$

We assume that the volume flows satisfy $Q_F(t) \geq 0$, $Q_r(t) \geq 0$ and $Q_l(t) \leq 0$. Dividing (3.1) by $S$ shows that

$$q(x,t) = \begin{cases} q_l(t) = q_r(t) - Q_F(t)/S \leq 0 & \text{for } x < 0, \\ q_r(t) \geq 0 & \text{for } x > 0. \end{cases} \tag{3.2}$$

The prescribed local volumetric solids concentration of the feed flux is $u_F(t)$. Consequently, the solids continuity equation for $-1 < x < 1$ can formally be written as

$$u_t + \big(q(x,t)u + h(u)\big)_x = \delta(x)\frac{Q_F(t)u_F(t)}{S}, \tag{3.3}$$

where $\delta$ denotes the Dirac unit mass located at $x = 0$, and $q(x,t)$ is given by (3.2). Expressing $\delta$ as the derivative of the Heaviside function $H$ (defined by $H(x) = 1$ for $x > 1$ and $H(x) = 0$ otherwise) and noting that

$$q(x,t) = q_l(t) + H(x)(q_r(t) - q_l(t)) = q_l(t) + H(x)\frac{Q_F(t)}{S},$$

we can rewrite Eq. (3.3) as

$$u_t + \big(q(x,t)\big(u - u_F(t)\big) + q_l(t)u_F(t) + h(u)\big)_x = 0.$$

Taking into account that the Kynch batch flux density function $h$ is zero outside the interval $(-1,1)$, we finally obtain the hyperbolic conservation law

$$u_t + g(x,t,u)_x = 0, \quad -\infty < x < \infty,\ t > 0 \tag{3.4}$$

with the composite flux density function

$$g(x,t,u) = \begin{cases} q_l(t)u & \text{for } x < -1, \\ q_l(t)u + h(u) & \text{for } -1 < x < 0, \\ q_r(t)u + h(u) + \big(q_l(t) - q_r(t)\big)u_F(t) & \text{for } 0 < x < 1, \\ q_r(t)u + \big(q_l(t) - q_r(t)\big)u_F(t) & \text{for } x > 1. \end{cases} \tag{3.5}$$

For the remainder of this paper we regard $q_l(t)$, $q_r(t)$ and $u_F(t)$ as independent control variables satisfying $q_l(t) \leq 0$, $q_r(t) \geq 0$ (then we always have $Q_F(t) = S(q_r(t) - q_l(t)) \geq 0$) and $0 \leq u_F(t) \leq 1$. We shall also also assume that the control variables $q_l$, $q_r$ and $0 \leq u_F \leq 1$ are constant with respect

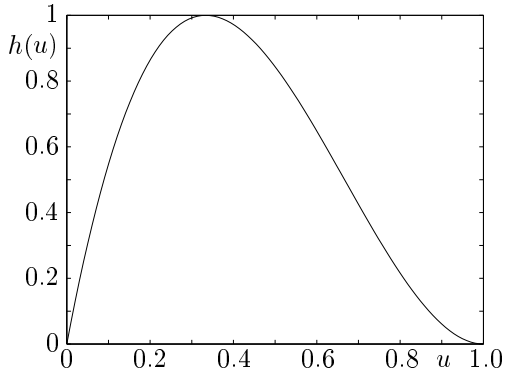


FIGURE 2. The Kynch batch flux density function $h(u) = \frac{27}{4}u(1-u)^2$.

to $t$, which also handles the practically relevant case of piecewise constant (with respect to $t$) data. Thus the model we consider is the following initial value problem:

$$\begin{aligned} u_t + g(x,u)_x = 0, \quad -\infty < x < \infty,\ t > 0, \\ u(x,0) = u_0(x), \quad -\infty < x < \infty, \end{aligned} \tag{3.6}$$

where, in view of (3.5), $g(x,u)$ has its obvious meaning. By a solution $u$ we understand a weak solution, which is allowed to have discontinuities. This means we do not require that $u$ and its derivatives satisfy the partial differential equation $u_t + g(x,u)_x = 0$ in a pointwise sense. Rather, we multiply this equation by a sufficiently smooth test function $\varphi$, integrate over $(-\infty,\infty)\times(0,\infty)$, use integration by parts to move the derivatives from the solution to the test function, and require the resulting equation to hold for all test functions from a suitably chosen space. Here, the weak formulation reads as follows:

$$\int_{-\infty}^{\infty}\int_{0}^{\infty} \big(u\varphi_t + g(x,u)\varphi_x\big)\,dtdx + \int_{-\infty}^{\infty} u_0(x)\varphi(x,0)\ dx = 0 \tag{3.7}$$

for all test functions $\varphi \in C_0^\infty(\mathbb{R}\times[0,\infty))$. In Bürger *et al.* (2001), we demonstrated that there exists a weak solution to the initial value problem (3.6). The problem of existence of a solution to (3.6) had been left open after the work in (Diehl 1995, 1996, 1997, 2000, 2001).

The flux function $g$ is defined according to (3.5) by

$$g(x,u) = \begin{cases} q_l u & \text{for } x < -1, \\ f\big(q(x),u\big) & \text{for } -1 < x < 1, \\ q_r u + (q_l - q_r)u_{\mathrm{F}} & \text{for } x > 1. \end{cases} \tag{3.8}$$

The "interior" flux function $f$ is defined as

$$f(q,u) = q\,(u - u_{\mathrm{F}}) + h(u) + q_l u_{\mathrm{F}}. \tag{3.9}$$

For the plots and numerical examples in this paper we have used the following Kynch batch flux density function (see Figure 2):

$$h(u) = \frac{27}{4}\,u(1-u)^2. \tag{3.10}$$

## 4. The front tracking method

The clarifier-thickener model derived in Section 3 leads to three non-standard Riemann problems that need to be solved. The solutions of these problems are constructed in Section 4.1. Equipped with the Riemann solutions, we formulate in Section 4.2 the front tracking method for the clarifier-thickener model. The front tracking method presented here is also used in Bürger *et al.* (2001) to prove that there exists a weak solution to the clarifier-thickener model. This analysis is reviewed in Section 4.3.

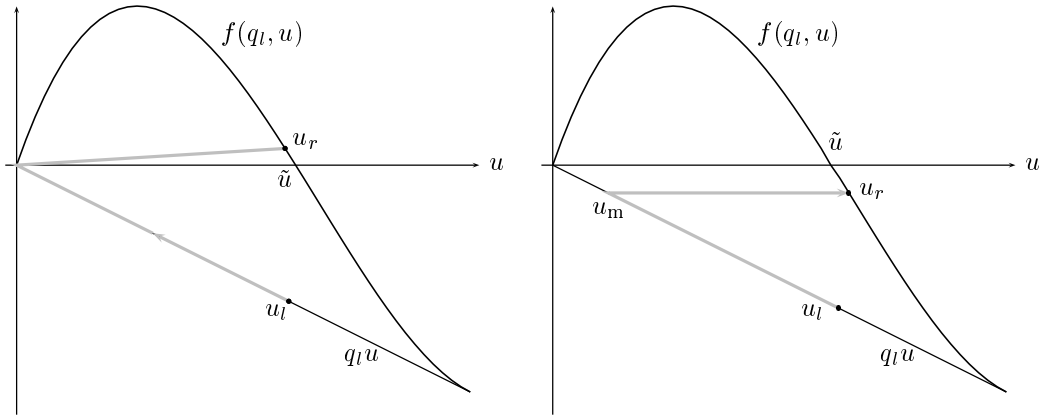


FIGURE 3. Construction of the solution of the Riemann problem (4.1) centered at $x = -1$ with $u_r < \tilde{u}$ (left) and $u_r \geq \tilde{u}$ (right).

4.1. **Solutions of the Riemann problems.** Now we shall solve the Riemann problems at the discontinuities of $g(\cdot, u)$. In this we follow Gimse and Risebro (1990), see also Bürger *et al.* (2001). First we describe the Riemann problems at the overflow and discharge levels $x = \mp 1$, each of which involves one linear and one nonlinear flux function.

At the overflow level $x = -1$, the left flux function is given by $f_l(u) = q_l u$ and the right flux function given by (3.9) with $q = q_l$. Precisely, we wish to solve the initial value problem (3.6) around $x = -1$ and for small $t$ where

$$u_0(x) = \begin{cases} u_l & \text{for } x < -1, \\ u_r & \text{for } x > -1. \end{cases} \tag{4.1}$$

There are two cases to consider depending on the sign of $f(q_l, u_r)$. Let $\tilde{u}$ be defined by

$$f(q_l, \tilde{u}) = 0 \quad \text{and} \quad \tilde{u} > 0. \tag{4.2}$$

If $f(q_l, u_r) > 0$ or $u_r < \tilde{u}$, then the solution is given by a discontinuity moving to the left with speed $q_l$, separating $u_l$ and 0, and a discontinuity moving to the right with speed $f(q_l, u_r)/u_r$, separating the values 0 and $u_r$. If $u_r > \tilde{u}$, let $u_\mathrm{m}$ be given by $u_\mathrm{m} = f(q_l, u_r)/q_l$ (see Figure 3). Then the solution is given by a discontinuity moving to the left with speed $q_l$, separating $u_l$ and $u_\mathrm{m}$, and a discontinuity located at $x = -1$ separating $u_\mathrm{m}$ and $u_r$. These two cases are shown in Figure 3.

For $x = 1$ the situation is slightly different since $f(q_r, u)$ can have both a local maximum and a local minimum for $u$ between 0 and 1. Now we wish to solve the Riemann problem defined by the initial datum

$$u_0(x) = \begin{cases} u_l & \text{for } x < 1, \\ u_r & \text{for } x > 1. \end{cases} \tag{4.3}$$

Let $f_\mathrm{min}$ denote the value at the local minimum, and $\bar{u}$ the corresponding $u$ value, i.e.,

$$f(q_r, \bar{u}) = f_\mathrm{min}, \tag{4.4}$$

and define $\underline{u}$ to be the unique solution of

$$f(q_r, \underline{u}) = f_\mathrm{min}, \tag{4.5}$$

where $\underline{u} < \bar{u}$. Then the solution of the Riemann problem depends on whether $u_l$ is in the interval $(\underline{u}, \bar{u})$ or not. If $u_l \in (\underline{u}, \bar{u})$, then the solution is given by a composite $u$ wave from $u_l$ to $\bar{u}$, followed by a $q$ wave with zero speed from $\bar{u}$ to $u_\mathrm{m}$, and then by a wave with speed $q_r$ from $u_\mathrm{m}$ to $u_r$. Here

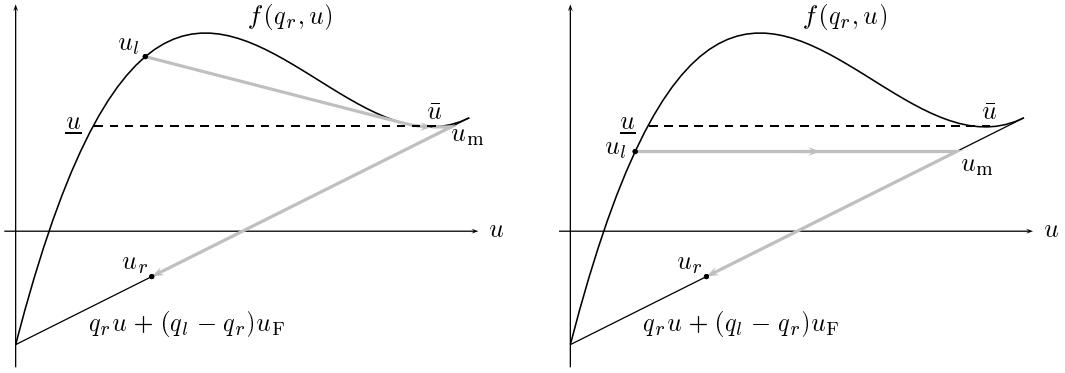


FIGURE 4. Construction of the solution of the Riemann problem (4.3) centered at $x = 1$ with $u_l \in (\underline{u}, \bar{u})$ (left) and $u_l \notin (\underline{u}, \bar{u})$ (right).

the term "composite wave" means a wave consisting of a shock followed by a rarefaction. The right middle state $u_{\mathrm{m}}$ is given by

$$u_{\mathrm{m}} = \frac{f_{\min} + (q_r - q_l)u_{\mathrm{F}}}{q_r}.$$

If $u_l \notin (\underline{u}, \bar{u})$, the solution is similar to the second case at $x = -1$. Now the solution is given by a $q$ wave of zero speed from $u_r$ to $u_{\mathrm{m}}$, followed by a right wave of speed $q_r$ from $u_{\mathrm{m}}$ to $u_r$. In this case the middle state $u_{\mathrm{m}}$ is given by

$$u_{\mathrm{m}} = \frac{f\,(q_r, u_l) + (q_r - q_l)u_{\mathrm{F}}}{q_r}.$$

Note that the state immediately to the left $x = 1$ is always in the set $[0, \underline{u}] \cup [\bar{u}, 1]$. See Figure 4 for an illustration. For later use we shall refer to the waves moving out of the interval $[-1, 1]$ as *left* and *right* waves respectively. The waves with zero speed sitting at $x = \mp 1$ we call left or right *boundary* waves. The waves moving into the region $[-1, 1]$ we label $u$ waves.

The Riemann problem defined by the discontinuity in $q$ at $x = 0$, which includes the feed mechanism, involves two nonlinear flux functions on either side and is therefore more complicated, but also covered by the general theory in by Gimse and Risebro (1990). This Riemann problem is given by

$$u_t + f(q,u)_x = 0, \tag{4.6}$$

$$u(x,0) = \begin{cases} u_l & \text{for } x < 0, \\ u_r & \text{for } x > 0, \end{cases} \qquad q(x) = \begin{cases} q_l & \text{for } x < 0, \\ q_r & \text{for } x > 0, \end{cases} \tag{4.7}$$

where $q_l \le 0 \le q_r$. We here demonstrate that there exists a unique entropy solution for all $u_l$ and $u_r$ in $[0, 1]$, in the sense that this solution is the limit of a viscous approximation. This solution consists of $u$ waves, over which $q$ is constant, and a $q$ wave, separating $q_l$ and $q_r$.

For simplicity, we shall assume that $f(q,u)$ is strictly monotone along the transition curve $T := \{(u,q) : \partial_u f(q,u) = 0\}$, which is the curve in the $(u,q)$-plane that joins the local extrema of $f(q,\cdot)$ with respect to $u$, see Figure 5. This means that the control parameters $q_l$, $q_r$ and $u_{\mathrm{F}}$ are chosen in such a way that $\partial_q f \neq 0$ on $T$, which then implies that either $u - u_{\mathrm{F}} < 0$ or $u - u_{\mathrm{F}} > 0$ on $T$.

We assume that the left inequality holds on the left branch of the transition curve, and the right inequality holds on the right branch. Furthermore, we shall assume that $q_r$ is so small that $f(q_r,u)$ has *both* a local maximum and a local minimum in $(0,1)$. We set $\bar{q}$ to be the largest value of $q_r$ for which this is the case. If $h(u)$ is chosen as (3.10) we find that $\bar{q} = 9/4$. Thus in this case we have the following restrictions on $u_{\mathrm{F}}$:

$$q_r < \frac{9}{4}, \quad \text{and} \quad \frac{2 - \sqrt{1 - 4q_r/9}}{3} < u_{\mathrm{F}} < \frac{2 + \sqrt{1 - 4q_r/9}}{3}. \tag{4.8}$$

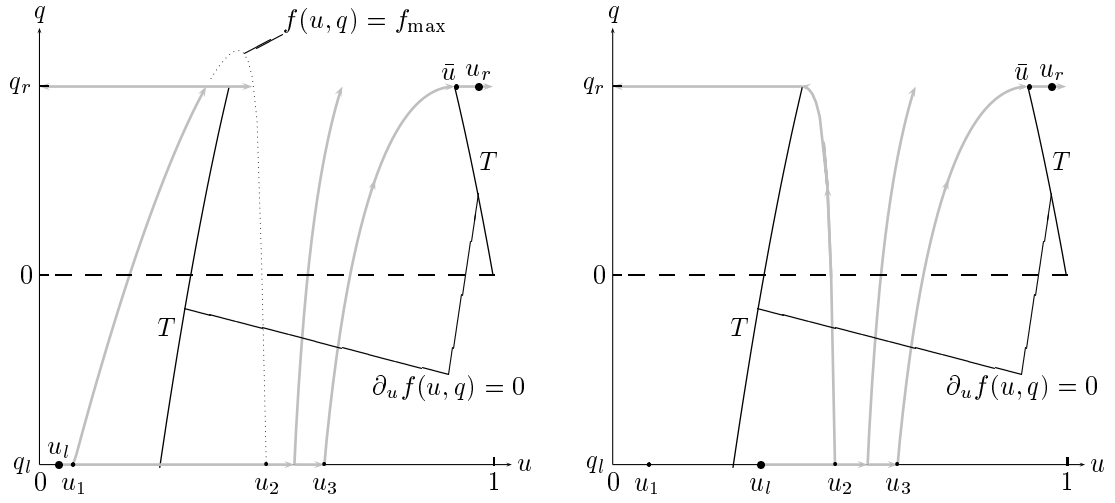


FIGURE 5. Solution of the Riemann problem (4.6) located at $x = 0$ with $u_l < u_1$ (left) and $u_l \geq u_1$ (right).

The restrictions (4.8) are inessential and stated for convenience only, since they give fewer cases to discuss when solving the Riemann problem at $x = 0$.

For later use we depict this solution in the $(u, q)$ plane, see Figure 5. We start at a point $(u_l, q_l)$ on the line $q_l \times [0, 1]$ and move on a gray path to the point $(u_r, q_r)$. There are two cases to consider depending on the location of $u_l$. Let $f_{\max}$ be the local maximum of $f(q_r, u)$ (such a maximum exists for $q_r < \bar{q}$), and let $u_1 < u_2$ denote the solutions of

$$f(q_l, u_1) = f(q_l, u_2) = f_{\max}. \tag{4.9}$$

The set of all points $(u, q)$ satisfying $f(q, u) = f_{\max}$ is shown as a dotted curve in Figure 5. Similarly, if $f(q_r, u)$ has a local minimum in $u$, then we let $f_{\min}$ denote this value, and let $u_3$ be the unique solution of

$$f(q_l, u_3) = f_{\min}. \tag{4.10}$$

The solution path is depicted as a gray path in the figures. The horizontal segments are $u$ waves while the segments that move on contour lines of $f(q, u)$ are $q$ waves. To find a particular solution, follow the gray path from $(q_l, u_l)$ (on the lower horizontal line) in the direction of the arrows to the any point $(q_r, u_r)$.

For example, assume that $u_l < u_1$, i.e., we are in the first case, and that $u_r$ lies to the right of the local minimum. Then the solution is given by a $u$ wave connecting $u_l$ and $u_3$, followed by a $q$ wave connecting $(u_3, q_l)$ with the local minimum, given by the point $\bar{u}$, where $\bar{u}$ is defined by (4.4), where the right branch of $T$ intersects the line $q = q_r$, and finally a $u$ wave connecting the $\bar{u}$ to $u_r$.

As another example consider the case where $u_l$ is between $u_1$ and $u_2$, and $u_r$ is to the left of the local maximum of $f(q_r, u)$. Then, according to the right part of Figure 5, the solution consists of a $u$ wave from $u_l$ to $u_2$ (this wave will be a shock wave), followed by a $q$ wave connecting $(u_l, q_l)$ with $(\hat{u}, q_r)$, where $\hat{u}$ is the local maximum of $f(q_r, u)$, followed by $u$ wave from $\hat{u}$ to $u_r$ (this wave will be a rarefaction).

Finally, we mention that any Riemann problems occurring inside the intervals $(-1, 0)$ or $(0, 1)$ are Riemann problems for a single scalar conservation law, and are solved by taking the envelope of the flux function, see Holden and Risebro (2001) and Chapter 5 of Bustos *et al.* (1999). Riemann problems outside the interval $[-1, 1]$ are Riemann problems for a linear equation, and their solution is trivial.

4.2. **The front tracking procedure.** Now that we have determined the solutions of all non-standard Riemann problems occurring in our application, we can employ them as a tool for constructing approximations to more general Cauchy problems. The front tracking algorithm we construct closely resembles the ones used by Gimse and Risebro (1992) and Klingenberg and Risebro (1995, 2001). These algorithms are all based on the fact that for a scalar conservation law of the form (2.1), one can construct the exact entropy solution if $\phi$ is piecewise linear on a finite number of intervals, and $u_0$ takes values in the set of breakpoints of $\phi$ (Holden *et al.* 1988). Such an algorithm was also presented by Bustos and Concha (1999). We shall make piecewise linear (in $u$) approximations to $f(q_l,u)$ and $f\,(q_r,u)$ in such a way that the solution of the Riemann problem at $x=0$ is easy to compute.

To be specific, choose a (small) positive number $\delta$. Let $\bar{u}_1$ and $\bar{u}_2$ denote the local extrema of $f\,(q_r,u)$. For $i=0,\mp1,\mp2,\ldots$ let $u_i(q)$ denote the solutions of

$$f\big(q,u_i(q)\big)=f_i,\quad f_i=i\delta. \tag{4.11}$$

In other words, the curves $u_i(q)$ are the contour lines of $f$ in the $(u,q)$-plane.

With a slight abuse of notation, we define for $q=q_l$ and $q=q_r$ the finite sets of points

$$\{u_i(q_r)\}=\{0,\bar{u}_1,\bar{u}_2,1\}\cup\{u_i(q_r)\}\cap[0,1],\quad \{u_i(q_l)\}=\{0,u_1,u_2,u_3,1\}\cup\{u_i(q_l)\}\cap[0,1],$$

where $u_1$, $u_2$ and $u_3$ are defined by (4.9) and (4.10):

$$f(q_l,u_1)=f(q_l,u_2)=f(q_r,\hat{u})=f_{\max}\quad\text{and}\quad f(q_l,u_3)=f(q_r,\bar{u})=f_{\min},$$

see also Figure 5. We order the set $\{u_j(q)\}$ so that $u_{j-1}(q)<u_j(q)$. Then we define a piecewise linear (in $u$) approximation to $f(q,u)$ by

$$f^\delta(q,u)=f\,(q,u_j(q))+(u-u_j(q))\,\frac{f\,(q,u_{j+1}(q))-f\,(q,u_j(q))}{u_{j+1}(q)-u_j(q)}\quad\text{for } u\in[u_j(q),u_{j+1}(q)], \tag{4.12}$$

for $q=q_l$ or $q_r$. Note that for a fixed (constant) $q$, the entropy solution of the initial value problem

$$\begin{gathered}u_t+f^\delta(q,u)_x=0,\quad -\infty<x<\infty,\ t>0;\\ u(x,0)=u_0(x),\quad -\infty<x<\infty.\end{gathered}$$

can be found by front tracking if $u_0$ is piecewise constant, see Holden *et al.* (1988). Furthermore, if $u_0$ takes values in the set $\{u_i\}$, the solution will also take values in this set.

Note also that by construction of $f^\delta$, the solution of the Riemann problems in case $f$ is replaced by $f^\delta$, can still be described by Figure 5 for $x=0$ and by Figures 3 and 4 for $x=\mp1$. The breakpoints of $f^\delta$ are also chosen such that if for some $j$ the points $(q_l,u_j)$ are connected to $(q_r,u)$ by a $q$ wave, then $u\in\{u_i\}$. This means that if $u_j$ and $u_k$ are breakpoints, the solution of the Riemann problem

$$\begin{cases}u_t+f^\delta\,(q_l,u)_x=0, & u(x,0)=u_j\quad\text{for } x<0,\\ u_t+f^\delta\,(q_r,u)_x=0, & u(x,0)=u_k\quad\text{for } x>0\end{cases}$$

will take values among the breakpoints. Also, since the flux function is linear outside $[-1,1]$, then a similar observation is valid for Riemann problems defined at $x=\mp1$. Since $f^\delta$ is piecewise linear, the solutions of these Riemann problems will be piecewise constant, and the discontinuities will move with finite speed.

Now we are ready to define the front tracking approximation to (3.6). Let

$$g^\delta(x,u)=\begin{cases}q_l u & \text{for } x<-1,\\ f^\delta(q,u) & \text{for } -1<x<1,\\ q_r u+(q_l-q_r)u_{\mathrm{F}} & \text{for } 1<x,\end{cases} \tag{4.13}$$

and let $u_0^\delta(x)$ be a piecewise constant approximation to $u_0$ taking values in the set $\{u_i\}$. We define $u^\delta$ to be the weak solution to the polygonal initial value problem

$$\begin{gathered}u_t^\delta+g^\delta\left(x,u^\delta\right)_x=0,\quad -\infty<x<\infty,\ t>0,\\ u^\delta(x,0)=u_0^\delta(x),\quad -\infty<x<\infty.\end{gathered} \tag{4.14}$$

The weak solution $u^\delta$ is constructed as follows: First solve the Riemann problems defined by the discontinuities of $u_0^\delta$ and at the points $x = \mp 1$ and $x = 0$. This will give a finite number of discontinuities emanating from the discontinuities of $u_0^\delta$, $x = \mp 1$ and $x = 0$. When these collide, solve the Riemann problem defined by the state to the left and right of the collision. This Riemann problem will be of the same type as the initial Riemann problems. Therefore we can continue this process for as many collisions as we like, see Holden *et al.* (1988) and Holden and Risebro (2001). In the next section, we shall see that there will only be a finite number of collisions for all $t > 0$, and hence $u^\delta$ can be defined for any $t$.

4.3. **Analysis of the front tracking method.** The main purpose of the present contribution is to draw attention to the practical value of the front tracking method for the simulation of continuous sedimentation processes. Nevertheless, the mathematical analysis of this method is necessary in order to show that the correct (physically relevant) weak solution is approximated as the discretization parameter $\delta$ goes to zero. This convergence property ensures that the numerical method is reliable and is hence important for the practitioner. We therefore briefly summarize some recent results of the mathematical analysis of the front tracking method applied to the settler-clarifier model. For details we refer to Bürger *et al.* (2001).

From the present description of the front tracking procedure for continuous sedimentation it is not obvious beforehand that the method is well-defined. For example, the collision of two discontinuities gives rise to a Riemann problem whose solution can result in a new fan of discontinuities, which in turn might produce new collisions and thereby could lead to an infinite number of discontinuities, such that the solution procedure never ends. It is therefore necessary to explicitly demonstrate that this does not occur. To this end, first recall that for a fixed time $t$, the approximate solution is piecewise constant, where the constant values belong to a finite set which is determined a priori through the piecewise linear approximations of the flux density functions. Consequently, requiring that the number of discontinuities of $u^\delta(\cdot, t)$ remains finite for all times is equivalent to stating that the *total variation* of $u^\delta(\cdot, t)$, defined as the sum of the absolute values of all jumps of $u^\delta(\cdot, t)$ (with respect to $x$ and $t$ fixed), remains bounded.

As in the papers by Gimse and Risebro (1992), Klingenberg and Risebro (1995, 2001) and Temple (1982), it is at least difficult (and perhaps impossible) to prove directly for the settler-clarifier problem that the total variation of $u^\delta(\cdot, t)$ remains finite. However, it is possible to show that the variation of a particular nonlinear functional of $u^\delta$, the so-called *Temple functional* $\Psi$ defined by

$$\Psi(q, u) = \int_0^u |\partial_u f(q, \xi)| \, d\xi + f(q, 0), \tag{4.15}$$

is bounded. Roughly speaking, the difference $\Psi(q_1, u_1) - \Psi(q_2, u_2)$ measures "how many" contour lines in a $q$ versus $u$ plot such as Figure 5 separate $(q_1, u_1)$ and $(q_2, u_2)$. To show that the total variation of $\Psi$ is bounded, observe that the front tracking solution can be viewed as a sequence of discontinuities or *fronts*, where we distinguish between left, left boundary, $q$, $u$, right boundary, and right fronts, corresponding to discontinuities that travel to the left of $x = -1$ (i.e., upwards), stationary discontinuities sitting at the discharge level $x = -1$, stationary discontinuities located at the feed level $x = 0$, the "conventional" jumps of the solution involving one nonlinear flux function of $u$ only, the stationary discontinuities at the overflow level $x = 1$, and the jumps traveling to the right of $x = 1$ (i.e., downwards), respectively. It is possible to define the *strength* $F$ for each type of fronts such that the strength majorizes the variation of the Temple functional. The strength $F(u^\delta(\cdot, t))$ of the front tracking approximation or *wave path* $u^\delta(\cdot, t)$ (as a function of $t$) is then simply defined as the sum of all strengths of the different types of fronts involved.

The strength has an important property in conjunction with the front tracking method. Consider the states $w_l = (q_l, u_l)$ and $w_r = (q_r, u_r)$ and assume that $[w_l, w_r]$ is the wave path obtained from appropriately solving the Riemann problem with left and right states given by $w_l$ and $w_r$, respectively. If $\gamma$ is any other wave path connecting $w_l$ and $w_r$, then $F([w_l, w_r]) \le F(\gamma)$. Bürger *et al.* (2001) establish this minimizing property by a careful discussion of the solution of each of the different types of Riemann problems involved. An additional inspection of the Riemann problems occurring due to collisions of the different fronts then reveals that the total variation of the Temple

functional is uniformly bounded by a constant which is independent of time and the discretization parameter $\delta$, and indeed decreased by at least $\delta$ each time a front is "reflected" from one of the boundary fronts. Since on the other hand $F \geq 0$ by definition, such collisions can take place only a finite number of times. For every fixed discretization parameter $\delta$, the front tracking method leads to an approximate solution $u^\delta$ which can be computed in a *finite* number of steps, since only a *finite* number of Riemann problems have to be solved and only a *finite* number of interactions occur.

With these statements it is obvious that the front tracking method is well-defined and leads within a finite number of steps to an approximate solution of the original initial value problem (3.6) for every fixed value of the discretization parameter $\delta$. In fact, $u^\delta$ is the *exact* weak solution of the *polygonal* and with reasonably small effort solvable initial value problem (4.14). Exploiting that $\Psi$ can be inverted, it is possible to prove that the family $\{u^\delta\}$ of front tracking solutions converges in an appropriate sense to a weak solution of the initial value problem (3.6), see Bürger *et al.* (2001) for further details.

## 5. A finite difference method

In this section we will describe another numerical method for the clarifier-thickener model. An advantage with this method is its simplicity. As we shall see, there is no need to solve complicated $2 \times 2$ Riemann problems (as is the case with the front tracking method). Moreover, the numerical method is given in terms of a very simple explicit updating formula (5.4) for advancing from one time level to the next. However, to achieve this simplicity we must to some extent sacrifice the superior accuracy of the front tracking method. We refer to Section 6 for numerical examples illustrating the qualitative difference between the front tracking method and the finite difference method.

We begin the construction of our finite difference method by discretizing the spatial domain $\mathbb{R} \equiv (-\infty, \infty)$ into cells

$$I_j = [x_{j-\frac{1}{2}}, x_{j+\frac{1}{2}}),$$

where $x_k = k\Delta x$ for $k = 0, \pm\frac{1}{2}, \pm 1, \pm\frac{3}{2}, \ldots$. Similarly, the time domain $[0, \infty)$ is discretized via $t_n = n\Delta t$ for $n = 0, 1, \ldots$, resulting in the time strips

$$I^n = [t_n, t_{n+1}).$$

Here $\Delta x > 0$ and $\Delta t > 0$ denote the spatial and temporal discretization parameters respectively.

Let $\chi_j(x)$ and $\chi^n(t)$ be the characteristic functions for the intervals $I_j$ and $I^n$, respectively, i.e.,

$$\chi_j(x) = \begin{cases} 1 & \text{if } x \in I_j, \\ 0 & \text{otherwise,} \end{cases} \qquad \chi^n(t) = \begin{cases} 1 & \text{if } t \in I^n, \\ 0 & \text{otherwise.} \end{cases}$$

Furthermore, define $\chi_j^n(x,t) = \chi_j(x)\chi^n(t)$ to be the characteristic function for the rectangle $I_j \times I^n$. We will use $U_j^n$ to denote the finite difference approximation of $u(j\Delta x, n\Delta t)$. The iteration (5.4) is started by setting

$$U_j^0 = \frac{1}{\Delta x} \int_{x_{j-\frac{1}{2}}}^{x_{j+\frac{1}{2}}} u_0(x)\, dx. \tag{5.1}$$

We view the flux $g(x,u)$ appearing in (3.6) as depending on two parameters $\gamma^1(x)$ and $\gamma^2(x)$, which we write as a vector for brevity:

$$\gamma(x) = \big(\gamma^1(x), \gamma^2(x)\big).$$

Then

$$g(x,u) := G(\gamma(x), u) := \gamma^1(x)(u - u_F) + \gamma^2(x)h(u) + q_l u_F,$$

with

$$\gamma^1(x) = \begin{cases} q_l & \text{for } x < 0, \\ q_r & \text{for } x > 0 \end{cases} \quad \text{and} \quad \gamma^2(x) = \begin{cases} 1 & \text{for } x \in (-1,1), \\ 0 & \text{for } x \notin (-1,1). \end{cases}$$

The parameter $\gamma^1(x)$ corresponds to the mixture flow velocity $q(x)$. The discontinuity at $x = 0$ is due to the separation between the clarification zone ($x < 0$) where the flow is upward ($q_l < 0$), and the settling zone ($x > 0$) where the flow is downward ($q_r > 0$).

The spatially varying flux parameter vector $\gamma$ is then discretized as follows:

$$\gamma_{j+\frac{1}{2}} = \frac{1}{\Delta x} \int_{x_j}^{x_{j+1}} \gamma(x)\, dx, \tag{5.2}$$

i.e., on a mesh that is *staggered* with respect to that of $u$.

The difference solution $\{U_j^n\}$ is extended to all of $\mathbb{R} \times [0, \infty)$ by defining

$$u^\Delta(x,t) = \sum_n \sum_j \chi_j^n(x,t) U_j^n, \qquad (x,t) \in \mathbb{R} \times [0,\infty), \tag{5.3}$$

where $\Delta = \Delta t = \lambda \Delta x$ and $\lambda$ is the mesh size ratio specified below. Similarly, the discrete parameter vector $\{\gamma_{j+\frac{1}{2}}\}$ is extended to all of $\mathbb{R}$ by defining

$$\gamma^\Delta(x) = \sum_j \chi_{j+\frac{1}{2}}(x) \gamma_{j+\frac{1}{2}}, \qquad x \in \mathbb{R},$$

where $\chi_{j+\frac{1}{2}}$ is the characteristic function for the interval $I_{j+\frac{1}{2}} = [x_j, x_{j+1})$.

The difference scheme takes the following conservation form

$$U_j^{n+1} = U_j^n - \lambda \Big( \bar{G}(\gamma_{j+\frac{1}{2}}, U_{j+1}^n, U_j^n) - \bar{G}(\gamma_{j-\frac{1}{2}}, U_j^n, U_{j-1}^n) \Big). \tag{5.4}$$

Here, the numerical flux $\bar{G}(\gamma, v, u)$ is the Engquist-Osher numerical flux, generalized slightly to accommodate the spatial variation of the flux $G(\gamma(x), u)$:

$$\bar{G}(\gamma, v, u) = \frac{1}{2}\big(G(\gamma, u) + G(\gamma, v)\big) - \frac{1}{2} \int_u^v |G_u(\gamma, w)|\, dw. \tag{5.5}$$

The Engquist-Osher numerical flux is consistent with the actual flux in the sense that

$$\bar{G}(\gamma, u, u) = G(\gamma, u).$$

In addition, for fixed $\gamma$, $\bar{G}(\gamma, v, u)$ is a two-point monotone flux, meaning that it is nonincreasing with respect to $v$, and nondecreasing with respect to $u$. In fact, the partial derivatives of the numerical flux satisfy

$$\min\big(0, G_u(\gamma, v)\big) = \bar{G}_v(\gamma, v, u) \le 0 \le \bar{G}_u(\gamma, v, u) = \max\big(0, G_u(\gamma, u)\big). \tag{5.6}$$

It is possible to show that for initial data $u_0(\cdot) \in [0, 1]$, if the parameter $\lambda$ is chosen so that the following CFL condition is satisfied

$$2\lambda \Big( \max(-q_l, q_r) + \max_u |h'(u)| \Big) \le 1, \tag{5.7}$$

then the computed solutions $U_j^n$ remain in the interval $[0, 1]$, the CFL condition (5.7) holds for each succeeding time step and the scheme (5.4) is monotone.

Using the fact that the numerical solution operator is monotone and conservative, it is possible to show that a discrete time continuity estimate holds:

$$\Delta x \sum_{j=-\infty}^{\infty} \big| U_j^{n+1} - U_j^n \big| \le \Delta x \sum_{j=-\infty}^{\infty} \big| U_j^1 - U_j^0 \big| \le C \Delta t. \tag{5.8}$$

Here the constant $C$ depends on the total variation of $u_0$ and $\gamma$, but not on the mesh refinement parameters $\Delta x$ and $\Delta t$.

As in the case of the front tracking algorithm, the critical ingredient in establishing convergence of the sequence of approximations $\{u^\Delta\}$ is a uniform bound on the spatial variation, as measured by a singular transformation. For the finite difference algorithm, we use the singular mapping

$$\Psi_{\mathrm{fd}}(\gamma, u) = \int_0^u |\partial_w G(\gamma, w)|\, dw. \tag{5.9}$$

It is possible to achieve such a uniform bound on the spatial variation by using the time continuity estimate (5.8), along with the discrete entropy inequalities satisfied by the Engquist-Osher scheme.

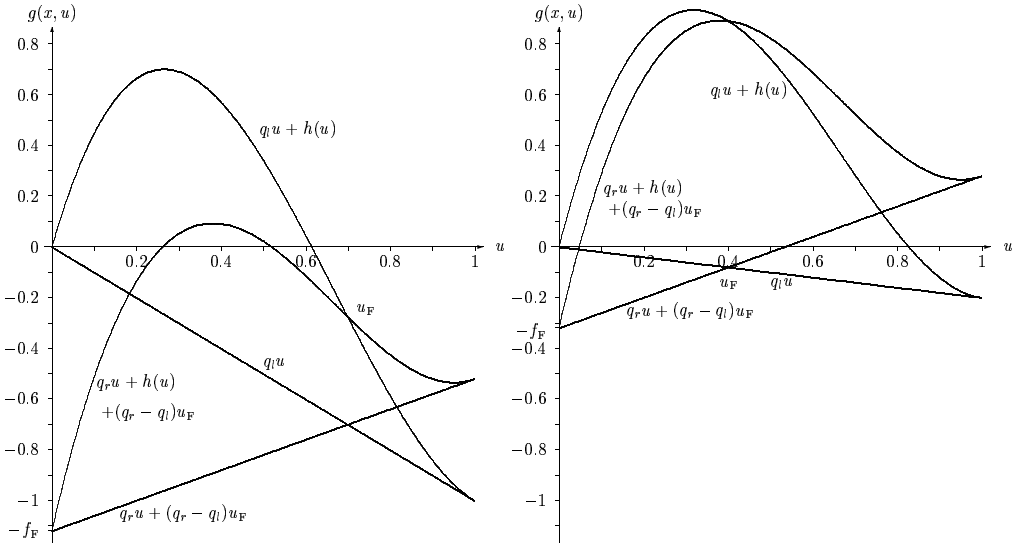


FIGURE 6. The flux density functions for Example 1 for $t \le 2.5$ (left) and $t > 2.5$ (right).

The proof depends in an essential way on the close functional relationships between the viscosity of the Engquist-Osher flux, the Kružkov entropy flux $F(\gamma, u) = \operatorname{sign}(u - c)\,(G(\gamma, u) - G(\gamma, c))$, and the singular mapping (5.9).

A detailed convergence proof for the finite difference method described herein will be presented in a forthcoming paper.

## 6. Numerical examples

We consider here two numerical examples to illustrate the numerical methods.

6.1. **Example 1 (front tracking method).** In the first example, we choose the initial and control functions

$$u_{\mathrm{F}} = \begin{cases} 0.7 & \text{for } t \le 2.5, \\ 0.4 & \text{for } t > 2.5, \end{cases}, \quad q_l = \begin{cases} -1 & \text{for } t \le 2.5, \\ -0.2 & \text{for } t > 2.5, \end{cases} \quad q_r = 0.6,$$

and initial data $u(x, 0) = 0$. The flux density functions for this case are plotted in Figure 6. Figure 7 shows the fronts generated by the front tracking method for this example, where the discretization parameter $\delta = 0.005$ is chosen. Figure 8 displays the same front tracking solution as a sequence of concentration profiles taken at various times. For $t \le 2.5$ the data of Example 1 are the same as in Example 1 of Bürger *et al.* (2001), but in that paper the discretization was chosen coarser ($\delta = 1/80$). The example shows how the clarifier-thickener is first filled up at a solids feed rate which exceeds the maximum possible solids discharge rate. Thus the sediment level rises above the feed level. Instead of letting the unit overflow, as in the simulation of Bürger *et al.* (2001), we drastically reduce the solids feed flux $f_{\mathrm{F}}$ but keep the discharge velocity $q_r$ constant. As a consequence the sediment level decreases and eventually the ideal clarifier-thickener unit empties. The change of flux density functions at $t = 2.5$ becomes visible in Figure 7 in that at that time several discontinuities split into two diverging fronts. The discussion of Sect. 4.3 has shown that this does not occur during the standard application of the front tracking method without changes of the flux density functions.

6.2. **Example 2 (front tracking method).** In the next example we study the way changes of the feed flux propagate into the thickening and clarification zones. We keep the discharge bulk flux constant at $q_r = 0.6$ and vary the values of $q_l$ and $u_{\mathrm{F}}$. This is done in such a way that the

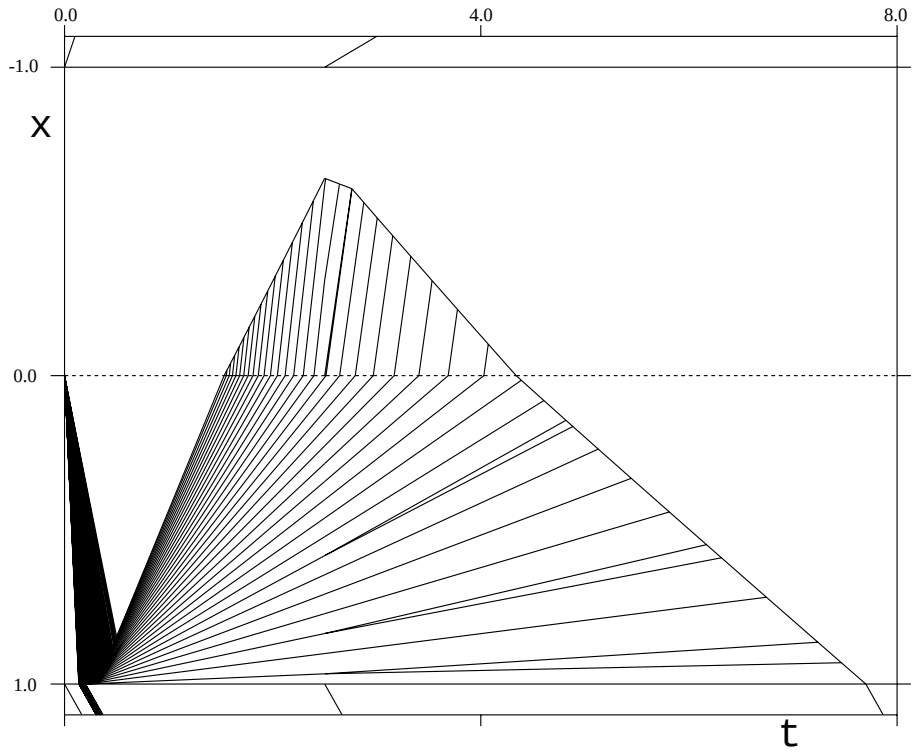


FIGURE 7. Example 1: Fronts calculated by the front tracking method with $\delta = 0.005$.

feed flux $f_{\mathrm{F}} = (q_r - q_l)u_{\mathrm{F}}$ is kept constant. Specifically, we choose

$$q_l = \begin{cases} -0.4 & \text{for } 0 \le t \le 1, \\ -0.6 & \text{for } 1 < t \le 3, \\ -0.9 & \text{for } 3 < t \le 5, \\ -0.2 & \text{for } t \ge 5, \end{cases} \qquad u_{\mathrm{F}} = \begin{cases} 0.6 & \text{for } 0 \le t \le 1, \\ 0.5 & \text{for } 1 < t \le 3, \\ 0.4 & \text{for } 3 < t \le 5, \\ 0.75 & \text{for } t \ge 5. \end{cases}$$

Observe that all values give $f_{\mathrm{F}} = 0.6$. Moreover we set initially $u_0 = 0.5$.

In Figure 9 we show the fronts resulting from a simulation with $\delta = 0.005$, in the time interval $[0, 20]$. At this time a stationary solution is not yet reached.

In Figure 10 we show the same numerical solution as concentration profiles at various times. We remark that a stationary solution, i.e., a steady state of continuous sedimentation, is reached at $t \approx 145$. The last diagram of Figure 10, corresponding to $t = 150.0$, shows the stationary state.

6.3. **Example 1 (finite difference method).** In Figures 11 to 14 we show the results of applying the finite difference scheme to Example 1. In all cases, we used $\Delta x = 0.02$ and $\Delta t = 0.0025$, i.e., both the clarification and thickening zones are subdivided into 50 cells. Each dot in Figures 11 to 17 illustrating the finite difference method corresponds to the solution value of one cell.

The overall solution pictures indicate that the finite difference scheme approximates the same solution as the front tracking method, as expected. The numerical examples illustrate the tendency of the finite difference scheme to 'smear out' discontinuities due to numerical viscosity. For example, Figures 13 (a) and (b) show several isolated dots near $x = -0.4$. This means that the upwards traveling concentration discontinuity, which is sharply resolved by the front tracking method (as seen in the lower left and middle diagrams of Figure 8) is smeared out over several computational cells.

6.4. **Example 2 (finite difference method).** In Figures 15 to 17 we show the results of running the finite difference scheme on Example 2. Here we used $\Delta x = 0.02$, $\Delta t = 0.0025$ for all runs,

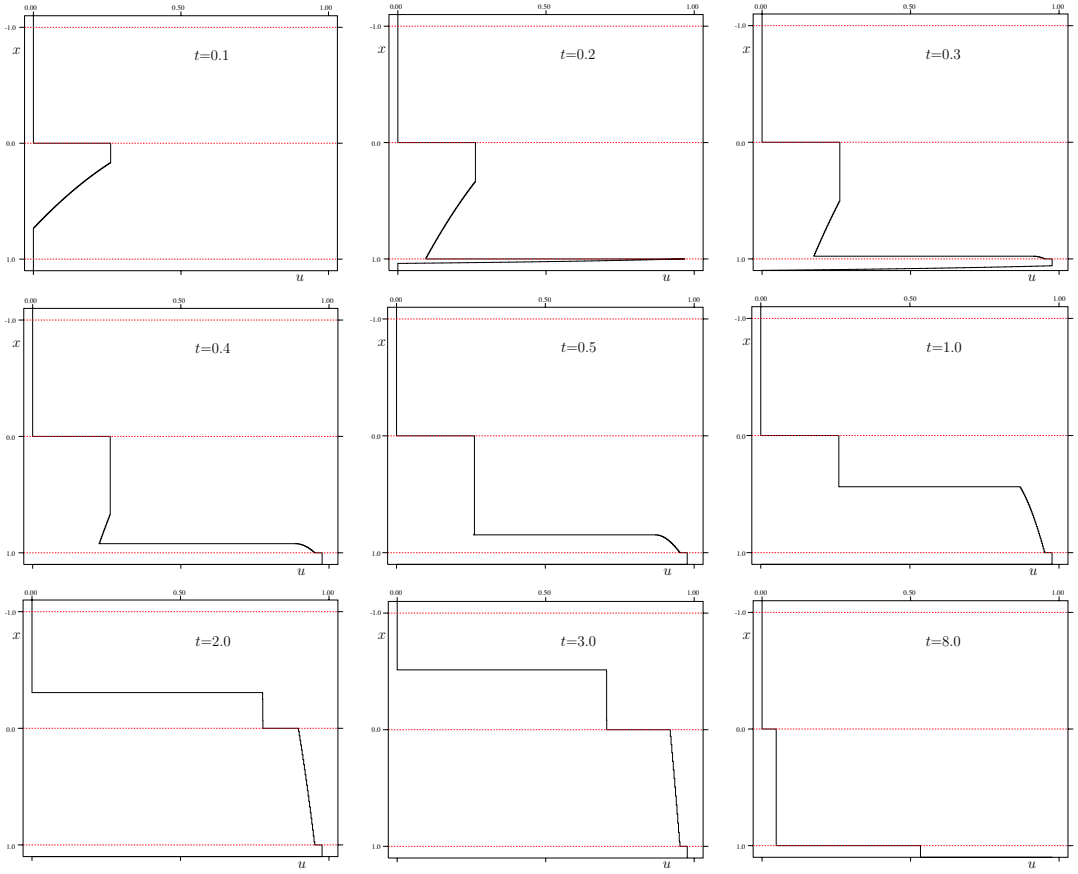


FIGURE 8. Example 1: Concentration profiles calculated by the front tracking method with $\delta = 0.005$.

with the exception of Figure 15 (b), which corresponds to $t = 0.6$. For this one run, we halved the mesh parameters to $\Delta x = 0.01$ and $\Delta t = 0.00125$ in order to resolve the small downward jump occurring at $x = 0$. With the coarser mesh, this feature did not appear at all.

The 'smearing' effect of the finite difference method is also visible in this example. For instance, compare Figure 15 (a) with the corresponding front tracking result, i.e., the upper left diagram of Figure 10.

## 7. Conclusions

The present work shows that ideal clarifier-thickener models proposed by several authors can be simulated accurately and efficiently by two alternative methods, an accurate and rapid front tracking method and a mildly disspative and somewhat slower, but very easily implemented finite difference method. The numerical examples show that despite their fundamentally different design principles, both schemes approximate the same solutions.

We emphasize that the mathematical analysis, providing a theoretical foundation of the reliability of the methods, is by no means trivial, despite the apparently simple clarifier-thickener setup, and based on very recent analyses (Bürger et al., 2001; Karlsen et al., 2001; Towers 2000, 2001). The essential main problem that had to be solved is of course the correct treatment of the feed level flux discontinuity located at $x = 0$. It is strongly emphasized that both methods regard the feed mechanism and the associated flux discontinuity as a *true* point source. It had not been obvious previously that this would be possible at all. This becomes apparent, for example, in the paper by Chancelier *et al.* (1994), who analysed a clarifier-thickener model that in the special case of a cylindrical vessel is equivalent to ours. However, they smooth out the discontinuities

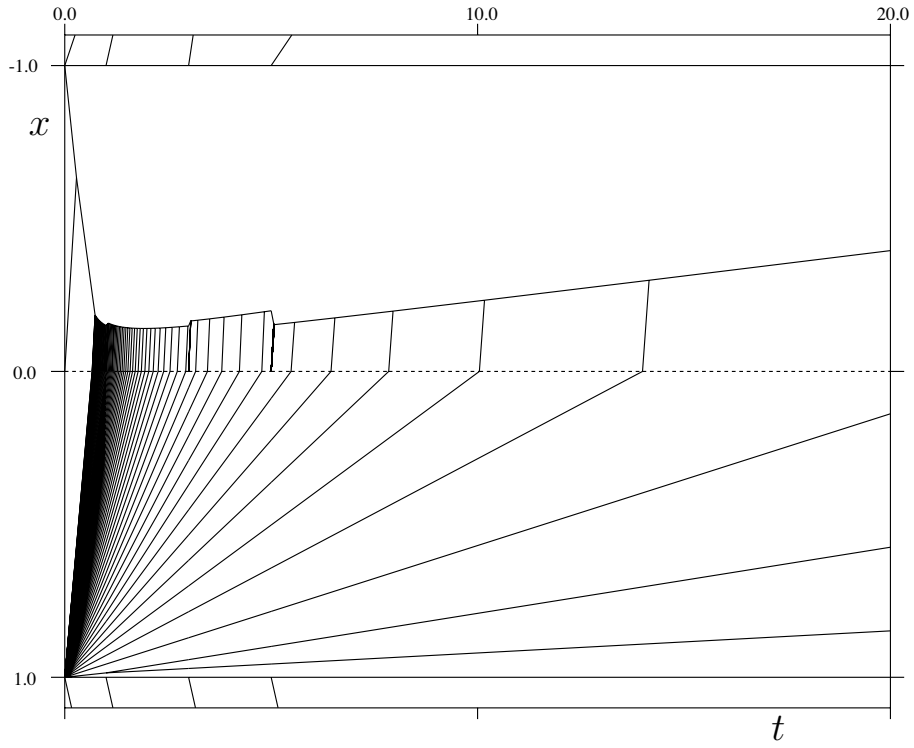


FIGURE 9. Example 2: Fronts calculated by the front tracking method with $\delta = 0.005$.

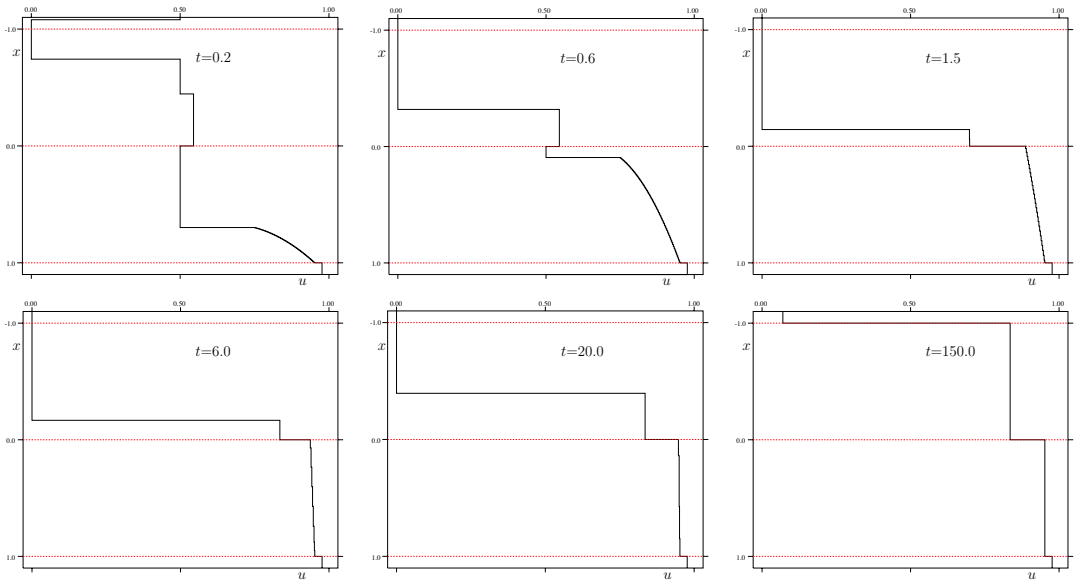


FIGURE 10. Example 2: Concentration profiles calculated by the front tracking method with $\delta = 0.005$. The last diagram (corresponding to $t = 150$ shows the steady state solution.

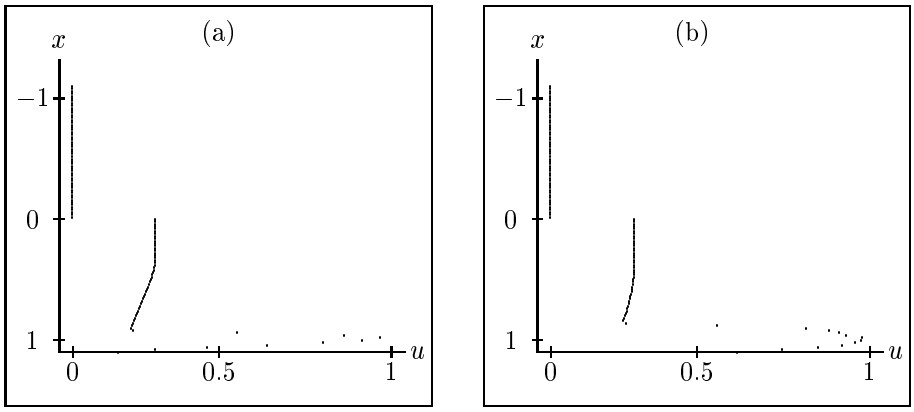


FIGURE 11. Example 1: Concentration profiles calculated by the finite difference method for (a) $t = 0.3$ (120 steps with $\Delta t = 0.0025$), (b) $t = 0.4$ (160 steps with $\Delta t = 0.0025$).

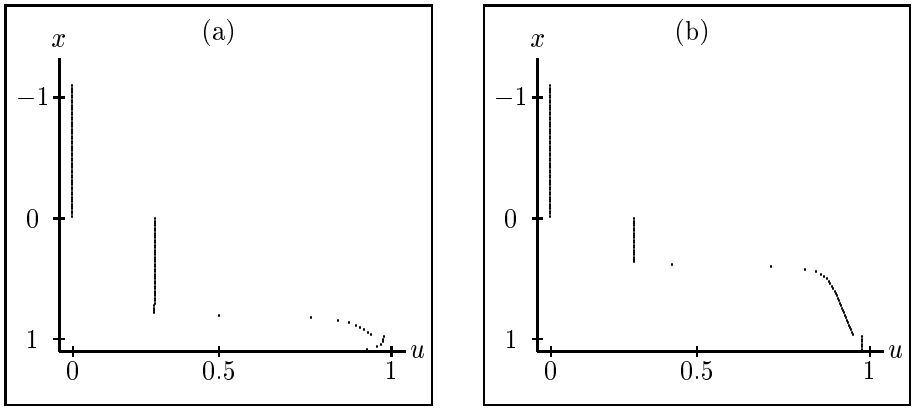


FIGURE 12. Example 1: Concentration profiles calculated by the finite difference method for Example 1 for (a) $t = 0.5$ (200 steps with $\Delta t = 0.0025$), (b) $t = 1.0$ (400 steps with $\Delta t = .0025$).

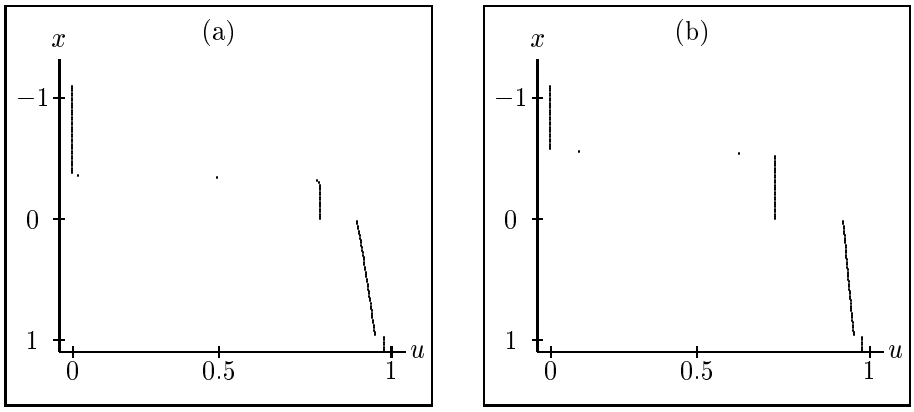


FIGURE 13. Example 1: Concentration profiles calculated by the finite difference method for (a) $t = 2.0$ (800 steps with $\Delta t = 0.0025$), (b) $t = 3.0$ (1200 steps with $\Delta t = 0.0025$).

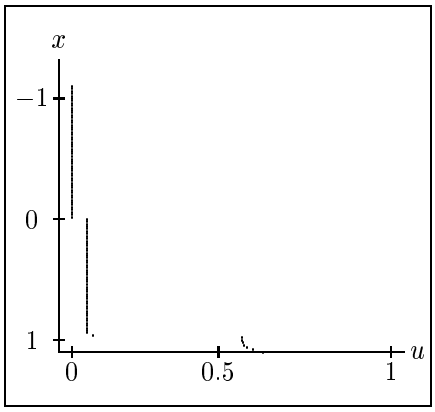


FIGURE 14. Example 1: Concentration profiles calculated by the finite difference method for $t = 8.0$ (3200 steps with $\Delta t = .0025$).

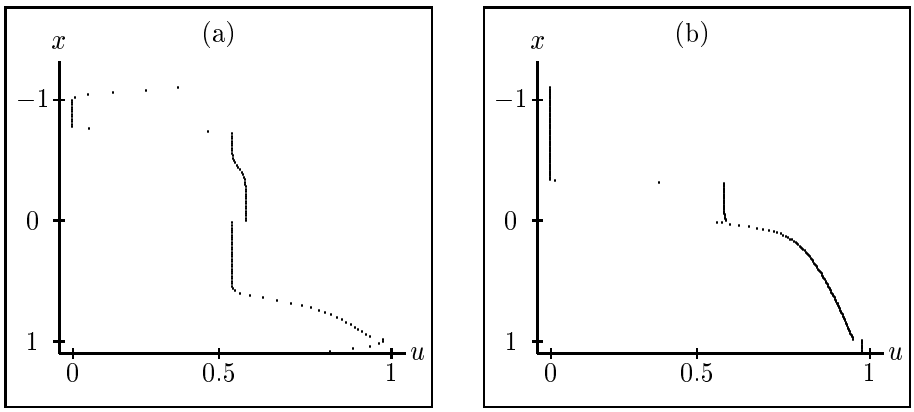


FIGURE 15. Example 2: Concentration profiles calculated by the finite difference method for (a) $t = 0.2$ (80 steps with $\Delta t = 0.0025$), (b) $t = 0.6$ (480 steps with $\Delta t = 0.00125$).

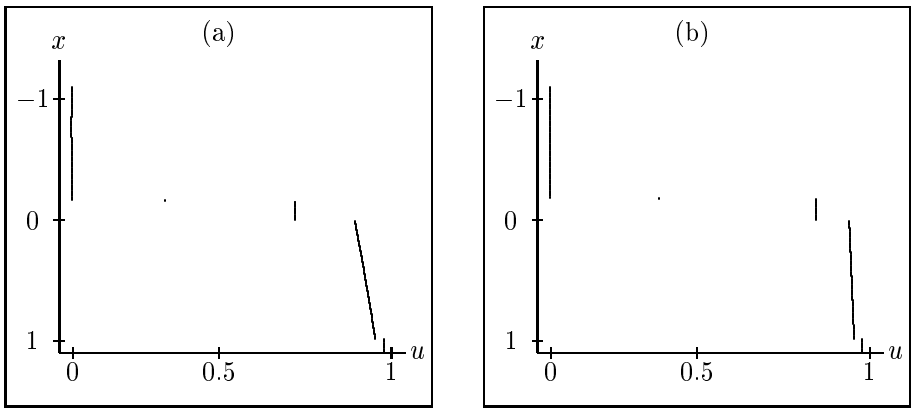


FIGURE 16. Example 2: Concentration profiles calculated by the finite difference method for (a) $t = 1.5$ (600 steps with $\Delta t = 0.0025$), (b) $t = 6.0$ (2400 steps with $\Delta t = 0.0025$).

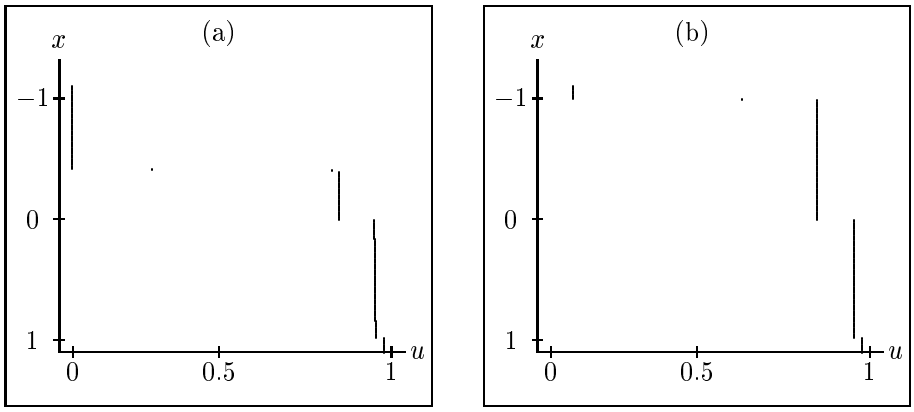


FIGURE 17. Example 2: Concentration profiles calculated by the finite difference methos for (a) $t = 20.0$ (8000 steps with $\Delta t = 0.0025$), (b) $t = 150.0$ (60000 steps with $\Delta t = 0.0025$).

of the discontinuous flux in order "to avoid technical difficulties" (p. 957) and continue to work with the "smoothed" problem, which can be expressed as a (harmless) conservation law with a smooth source term. In a similar manner, Barton et al. (1992) distribute the feed source in their numerical discretization over several cells. The present paper shows that these "difficulties" have not continued to be insurmountable and that such "smoothing" (although in many contexts widespread engineering practice) is unnecessary.

## ACKNOWLEDGMENTS

We acknowledge support by the Collaborative Research Program (Sonderforschungsbereich) 404 at the University of Stuttgart, the Applied Mathematics in Industrial Flow Problems (AMIF) program of the European Science Foundation (ESF), and the project *Nonlinear partial differential equations of evolution type - theory and numerics*, which is part of the BeMatA program of The Research Council of Norway.

## REFERENCES

Barton, N.G., Li, C.-H. and Spencer, S.J., 1992. Control of a surface of discontinuity in continuous thickeners. J. Austral. Math. Soc. Ser. B 33, 269–289.

Bressan, A., 1992. Global solutions to systems of conservation laws by wave-front tracking. J. Math. Anal. Appl. 170, 414–432.

Bürger, R., Karlsen, K.H., Klingenberg, C. and Risebro, N.H., 2001. A front tracking approach to a model of continuous sedimentation in ideal clarifier-thickener units. UCLA Computational and Applied Mathematics Report.

Bürger, R. and Tory, E.M., 2000. On upper rarefaction waves in batch settling. Powder Technol. 108, 74–87.

Bürger, R. and Wendland, W.L., 2001. Sedimentation and suspension flows: Historical perspective and some recent developments. J. Eng. Math. 41, 101–116.

Bustos, M.C. and Concha, F., 1999. Settling velocities of particulate systems: 10. A numerical method for solving Kynch sedimentation processes. Int. J. Mineral Process. 57, 185–203.

Bustos, M.C., Concha, F., Bürger, R. and Tory, E.M., 1999. *Sedimentation and Thickening.* Kluwer Academic Publishers, Dordrecht, The Netherlands.

Bustos, M.C., Concha, F. and Wendland, W.L., 1990. Global weak solutions to the problem of continuous sedimentation of an ideal suspension. Math. Meth. Appl. Sci. 13, 1–22.

Bustos, M.C., Paiva, F. and Wendland, W.L., 1996. Entropy boundary conditions in the theory of sedimentation of ideal suspension. Math. Meth. Appl. Sci. 19, 679–697.

Chancelier, J.P., Cohen de Lara, M. and Pacard, F., 1994. Analysis of a conservation PDE with discontinuous flux: a model of settler. SIAM J. Math. Appl. 54, 954–995.

Chang, D., Lee, T., Jang, Y., Kim, M. and Lee, S., 1997. Non-colloidal sedimentation compared with Kynch theory. Powder Technol. 92, 81–87.

Concha, F., Barrientos, A. and Bustos, M.C., 1995. Phenomenological model of high capacity thickening. In: Proc. of the *19th International Mineral Processing Congress (XIX IMPC)*, San Francisco 1995, Ch. 14, 75–79.

Concha, F. and Bustos, M.C., 1992. Settling velocities of particulate systems: 7. Kynch sedimentation processes: Continuous thickening. Int. J. Mineral Process. 34, 33–51.

Crandall, M.G. and Majda, A., 1980. Monotone difference approximations for scalar conservation laws. Math. Comp. 34, 1–21.

Dafermos, C.M., 1972. Polygonal approximations of solutions to the initial value problem for a conservation law. J. Math. Anal. Appl. 38, 33–41.

Dafermos, C.M., 2000. *Hyperbolic Conservation Laws in Continuum Physics.* Springer-Verlag, Berlin.

Davis, K.E., Russel, W.B. and Glantschnig, W.J., 1991. Settling suspensions of colloidal silica: observations and X-ray measurements. J. Chem. Soc. Faraday Trans. 87, 411–424.

Diehl, S., 1995. On scalar conservation laws with point source and discontinuous flux function. SIAM J. Math. Anal. 26, 1425–1451.

Diehl, S., 1996. A conservation law with point source and discontinuous flux function modelling continuous sedimentation. SIAM J. Math. Appl. 56, 388–419.

Diehl, S., 1997. Dynamic and steady-state behavior of continuous sedimentation. SIAM J. Appl. Math. 57, 991–1018.

Diehl, S., 2000. On boundary conditions and solutions for ideal thickener-clarifier units. Chem. Eng. J. 80, 119–133.

Diehl, S., 2001. Operating charts for continuous sedimentation I: control of steady states. J. Eng. Math. 41, 117–144.

DiPerna, R.J., 1976. Global existence of solutions to nonlinear systems of conservation laws. J. Diff. Eqns. 20, 187–212.

Engquist, B. and Osher, S., 1980. Stable and entropy satisfying approximations for transonic flow calculations. Math. Comp. 34, 45–75.

Gimse, T. and Risebro, N.H., 1990. Riemann problems with a discontinuous flux function. In: Proc. 3rd Conf. Hyp. Problems, Uppsala, Sweden, 1990.

Gimse, T. and Risebro, N.H., 1992. Solution of the Cauchy problem for a conservation law with a discontinuous flux function. SIAM J. Math. Anal. 23, 635–648.

Harten, A., Hyman, J.M, and Lax, P.D., 1976. On finite difference approximations and entropy conditions for shocks. Comm. Pure Appl. Math., 29, 297–322.

Holden, H., Holden, L. and Høegh-Krohn, R., 1988. A numerical method for first order nonlinear scaler conservation laws in one dimension. Comp. Math. Appl. 15, 595–602.

Holden, H. and Risebro, N.H., 2001. *Front Tracking For Conservation Laws.* Springer-Verlag, Berlin, to appear.

Karlsen, K.H., Risebro, N.H., and Towers, J.D, 2001. Convergence of an upwind difference scheme for degenerate parabolic convection-diffusion equations with a discontinuous flux. Preprint available at the URL www.math.ntnu.no/conservation/.

Klingenberg, C. and Risebro, N.H., 1995. Convex conservation laws with discontinuous coefficients. Comm. PDE 20, 1959–1990.

Klingenberg, C. and Risebro, N.H., 2001. Stability of a resonant system of conservation laws modeling polymer flow with gravitation. J. Diff. Eqns. 170, 344–380.

Kružkov, S.N., 1970. First order quasilinear equations in several independent variables. Math. USSR Sb. 10, 217–243.

Kunik, M., 1992. A numerical method for some initial-value problems of one scalar hyperbolic conservation law. Math. Meth. Appl. Sci. 15, 495–509.

Kunik, M., 1993. A solution formula for a non-convex scalar hyperbolic conservation law with monotone initial data. Math. Meth. Appl. Sci. 16, 895–902.

Kunik, M., Wendland, W.L., Paiva, F. and Bustos, M.C., 1993. The polygonal approximation in the Kynch theory of sedimentation. Technical Report 93-07, Department of Mathematical Engineering, University of Concepción, Chile.

Kynch, G.J., 1952. A theory of sedimentation. Trans. Faraday Soc. 48, 166–176.

Lev, O., Rubin, E. and Sheintuch, M., 1986. Steady state analysis of a continuous clarifier-thickener system, AIChE J. 32, 1516–1525.

Petty, C.A., 1975. Continuous sedimentation of a suspension with a nonconvex flux law. Chem. Eng. Sci. 30, 1451–1458.

Risebro, N.H., 1993. A front-tracking alternative to the random choice method. Proc. Amer. Math. Soc. 117, 1125–1139.

Severin, B.F., 1991. Clarifier sludge-blanket behavior at industrial activated-sludge plant. J. Env. Eng. 117, 718–730.

Shannon, P.T., Stroupe, E.P. and Tory, E.M., 1963. Batch and continuous thickening. Ind. Eng. Chem. Fund. 2, 203–211.

Shannon, P.T. and Tory, E.M., 1966. The analysis of continuous thickening. SME Trans. 235, 375–382.

Temple, B., 1982. Global solution of the Cauchy problem for a $2 \times 2$ non-strictly hyperbolic system of conservation laws. Adv. Appl. Math. 3, 335–375.

Tory, E.M., 1961. *Batch and Continuous Thickening of Slurries.* PhD Thesis, Purdue University, West Lafayette, IN, USA.

Towers, J.D., 2000. Convergence of a difference scheme for conservation laws with a discontinuous flux. SIAM J. Numer. Anal. 38, 681–698.

Towers, J.D., 2001. A difference scheme for conservation laws with a discontinuous flux - the nonconvex case. SIAM J. Numer. Anal. 39, 1197–1218.